

NASA Contractor Report 185259  
AIAA-90-1993

# Rocket Engine Failure Detection Using System Identification Techniques

Claudia M. Meyer and June F. Zakrajsek

*Sverdrup Technology, Inc.*  
*Lewis Research Center Group*  
*Brook Park, Ohio*

June 1990

Prepared for  
Lewis Research Center  
Under Contract NAS3-25266

**NASA**  
National Aeronautics and  
Space Administration

# ROCKET ENGINE FAILURE DETECTION USING SYSTEM IDENTIFICATION TECHNIQUES

Claudia M. Meyer and June F. Zakrajsek  
Sverdrup Technology, Inc.  
Lewis Research Center Group  
Brook Park, Ohio 44142

## Abstract

This paper presents the theoretical foundation and application of two univariate failure detection algorithms to Space Shuttle Main Engine (SSME) test firing data. Both algorithms were applied to data collected during steady-state operation of the engine. One algorithm, the time series algorithm, is based on time series techniques and involves the computation of autoregressive models. Time series techniques have been previously applied to SSME data. The second algorithm is based on standard signal processing techniques. It consists of tracking the variations in the average signal power with time. The average signal power algorithm is a newly proposed SSME failure detection algorithm. Seven nominal test firings were used to develop failure indication thresholds for each algorithm. These thresholds were tested using four anomalous firings and one additional nominal firing. Both algorithms provided significantly earlier failure indication times than did the current redline limit system. Neither algorithm gave false failure indications for the nominal firing. The strengths and weaknesses of the two algorithms are discussed and compared. The average signal power algorithm was found to have several advantages over the time series algorithm.

## Nomenclature

AR	autoregressive
ARMA	autoregressive moving average
CADS	command and data simulator
$e(t)$	unmeasurable disturbance
$E\{[x] \}$	mathematical expectation of a random process $x$
$f$	frequency in hertz
FPE	final prediction error
$g(k)$	coefficients of the transfer function $G(q)$
$G(q)$	transfer function from $u(t)$ to $y(t)$
$h(k)$	coefficients of the transfer function $H(q)$
$H(q)$	transfer function from $e(t)$ to $y(t)$
HPFP	high pressure fuel pump

HPFT	high pressure fuel turbine
HPFTP	high pressure fuel turbopump
HPOP	high pressure oxidizer pump
HPOT	high pressure oxidizer turbine
LPFP	low pressure fuel pump
LPOP	low pressure oxidizer pump
$m$	lag index
MCC	main combustion chamber
$p(x)$	probability density function of random variable $x$
$P_{xx}(f)$	power spectral density
PBP	preburner boost pump
PID	parameter identification
PSD	power spectral density
$q^{-1}$	shift operator
$r_{xx}[m]$	autocorrelation of a discrete stationary process at lag $m$
RPL	rated power level
SSME	space shuttle main engine
$T$	sampling interval in seconds
$u(t)$	input variable at time $t$
$x[n]$	discrete time function
$y(t)$	output variable at time $t$

## Introduction

An investigation was conducted to demonstrate the applicability of two steady-state failure detection algorithms to Space Shuttle Main Engine (SSME) data. One algorithm was based on time series techniques and the other on signal processing techniques. The algorithms were applied to improve the failure detection capability of safety systems during ground test firings and flight of the engine. With the current failure detection and control system on the SSME, several test firings have resulted in complete or partial loss of an engine. Forty-two firings have been classified as failures, and twenty-seven have had sufficient severity to be labeled as major failures.<sup>1</sup> The majority of these failures occurred during steady-state operation of the engine. Although this represents a small percentage of

the more than 1300 hot fire tests to date, these failures resulted in significant engine and facility damage, loss of fleet leader engine components, and a delay in the program schedule.

The current closed-loop SSME failure detection system employs basic redline limits. There are five redlined flight parameters; all monitor the high pressure turbopumps. These are the High Pressure Fuel Turbine (HPFT) and High Pressure Oxidizer Turbine (HPOT) discharge temperatures, the High Pressure Fuel Pump (HPFP) coolant liner pressure, the High Pressure Oxidizer Pump (HPOP) intermediate seal purge pressure, and the HPOT secondary seal cavity pressure. The redlined parameters have upper and/or lower limits assigned to them. Limit monitoring commences at scheduled times during startup and continues until the initiation of the shutdown phase.<sup>2</sup> The test firing failures described in Ref. 1 are evidence that a more advanced detection system is needed. The current limit monitoring techniques are not capable of detecting certain modes of failure with sufficient warning to avoid major hardware and facility damage. Significant improvements to safety would be realized by a system capable of detecting failures earlier than the current redline-based system.

Several advanced failure detection algorithms have been proposed for the SSME. To date, they have been tested off-line on past failures and nominal test firings and have demonstrated the ability to detect failures prior to the existing redline-limit system. One such algorithm, which monitors individual parameters during steady-state operation of the SSME, is the System for Anomaly and Failure Detection (SAFD) algorithm.<sup>3</sup> Another univariate approach which has been applied to steady-state SSME data is time series analysis.<sup>4</sup> Two multi-parameter algorithms have been proposed for improved steady-state failure detection. They are the Health Monitoring System for Rocket Engines (HMSRE) algorithm<sup>5</sup> and the clustering algorithm.<sup>4</sup> Finally, an approach developed to detect failures during non-steady-state operation of the SSME is the Recursive Structure Identification (RESID) technique.<sup>4</sup>

Two univariate failure detection algorithms were investigated and compared in this study. Both algorithms were employed during steady-state operation of the engine at 104 percent Rated Power Level (RPL) and 109 percent RPL. The algorithm based on time

series techniques had been previously reported and consisted of using Autoregressive (AR) models to predict the future behavior of parameters based on their past behavior. The time series algorithm was restricted to stationary signals because it involved the computation of models for signal prediction. Each model was computed over a 4-sec window, and errors between predicted and actual values were tracked over subsequent 4-sec windows. The second algorithm investigated, the average signal power algorithm, was based on a well-developed signal processing technique which has proven to be beneficial in all types of mechanical signature analysis.<sup>6</sup> The algorithm consisted of computing and tracking the average power of a signal over a 2-sec moving window. A smaller window was possible for the average signal power algorithm because this algorithm did not have model validity concerns. The smaller window decreased the time until the algorithm was available for failure detection. Furthermore, a stationary assumption could be made over the 2-sec computation window, allowing the average signal power algorithm to be applied to five more parameters than the time series algorithm. This paper presents the theoretical foundation of the time series and average signal power algorithms, and discusses their application to the SSME failure detection problem. The failure indication times of the two algorithms are presented, along with a comparison of the strengths and weaknesses of the algorithms.

The application of the time series algorithm and the average signal power algorithm was accomplished using a system identification and signal processing software package on a RISC workstation. Command and Data Simulator (CADS) data from seven nominal SSME tests were used to establish the failure indication thresholds for each algorithm. These tests were A2-457, A2-463, A2-479, A2-480, A2-481, A2-483, and A2-484. Both algorithms were tested with CADS data from four failures, A2-249, A1-340, A1-364, and A1-436, and one recent nominal test firing, A1-618. The first half of a test firing designation indicates the test stand on which the firing took place, and the second half indicates the test number. When the two algorithms were used in the failure detection mode, AR models were computed for 9 parameters, and the average signal power was computed for 14 parameters. The AR parameters were chosen because they typically displayed stationary behavior during steady-state operation of the engine. Furthermore, failure investigation summaries

indicated that some of the parameters chosen provided early failure indications for many of the anomalous test firings.<sup>2</sup> Parameters which were strongly affected by engine processes such as tank venting and pressurization could not be analyzed by either algorithm. The average signal power algorithm was applied to the one redlined parameter which was available in the four anomalous data sets and which met the above considerations. This parameter was the HPFT discharge temperature.

### Theory

#### Time Series Techniques

System identification is the process of selecting models created from experimental data that will represent the system or some of its properties. The approach generally followed is to model the system using measured input and output signals. In special cases where only single signals are recorded, a model is generated which will produce similar output when excited by white noise.

Generally, most applications of parametric estimation use discrete linear time series modeling techniques. This is due to Wold's fundamental theorem, which states that any stationary stochastic process can be expressed as the sum of two stationary and mutually uncorrelated processes.<sup>6</sup> For a general linear input-output configuration, a complete model description is given by

$$y(t) = G(q)u(t) + H(q)e(t) \quad (1)$$

where

$$G(q) = \sum_{k=1}^{\infty} g(k)q^{-k} \quad H(q) = 1 + \sum_{k=1}^{\infty} h(k)q^{-k} \quad (2)$$

and  $y(t)$  is the output signal,  $u(t)$  is the input signal, and  $e(t)$  is an unmeasurable disturbance into the system.<sup>7</sup>

The functions  $G$  and  $H$  are determined during modeling. To estimate these functions,  $G$  and  $H$  are parameterized as rational functions in the shift operator  $q^{-1}$ . By parameterizing Eq. (1), the general parametric model structure is given by

$$A(q)y(t) = \frac{B(q)}{F(q)}u(t) + \frac{C(q)}{D(q)}e(t) \quad (3)$$

where

$$\begin{aligned} A(q) &= 1 + a_1q^{-1} + \dots + a_{na}q^{-na} \\ B(q) &= b_1q^{-1} + b_2q^{-2} + \dots + b_{nb}q^{-nb} \\ C(q) &= 1 + c_1q^{-1} + \dots + c_{nc}q^{-nc} \\ D(q) &= 1 + d_1q^{-1} + \dots + d_{nd}q^{-nd} \\ F(q) &= 1 + f_1q^{-1} + \dots + f_{nf}q^{-nf} \end{aligned}$$

The orders of the polynomials are given by  $na$ ,  $nb$ ,  $nc$ ,  $nd$  and  $nf$ . For the AR model  $nc = nd = nf = 0$ , and  $C(q) = D(q) = F(q) = 1$ . Another commonly used model is the Autoregressive Moving Average (ARMA) model in which  $nd = nf = 0$  and  $D(q) = F(q) = 1$ .<sup>7</sup>

When there is no input into the system,  $u(t) = 0$ , the model given in Eq. 3 becomes

$$A(q)y(t) = C(q)e(t) \quad (4)$$

Equation (4) represents the general ARMA model structure for the case when no input is present. For the AR model,  $C(q) = 1$  in Eq. (4). These univariate models predict the behavior of a single parameter based upon the analysis of the past data of that parameter.  $C(q)$  is the moving average portion of the model, and attempts to describe the properties of the disturbance term,  $e(t)$ .<sup>7</sup>

The decision of which model type and order to select is a trade-off between implementation issues and the accuracy with which the model is able to describe the parameter. For example, in a real-time hardware implementation AR represents less computational burden than ARMA. Furthermore, for a given model type, lower order models can be computed more quickly. Therefore, given several models with similar prediction capabilities, the least complex model should be chosen.

The Final Prediction Error (FPE), a measure of the prediction capability of a model, simulates cross validation with another data set. The model with the smallest FPE should be chosen. The stability of the model is checked using a pole-zero diagram; all poles and zeros must lie within the unit circle. A near pole-zero cancellation indicates that a lower order model should be chosen. Also, if any of the uncertainty regions associated with the poles or zeros overlap, or cross the stability circle, a lower model order should be chosen. The frequency response comparison and the residual analysis are developed to determine the ability of the model to predict the data. The residuals between the actual data values and the modeled values should be random noise for the model to be a good predictor of the

system. This is checked by computing the autocorrelation function of the residuals.<sup>7</sup>

### Signal Processing Techniques

For discrete random processes, probabilistic functions are used to describe the behavior of the system. The mean or expected value of a random process at time  $n$  is given by Eq. (5):

$$\bar{x}[n] = \mathcal{E}\{x[n]\} \quad (5)$$

where

$$\mathcal{E}\{x\} = \int_{-\infty}^{\infty} xp(x)dx \quad (6)$$

and  $p(x)$  is the probability density function of  $x$ .

The autocorrelation function,  $r_{xx}[n_1, n_2]$ , of a random process at two different times  $n_1$  and  $n_2$  is defined as

$$r_{xx}[n_1, n_2] = \mathcal{E}\{x[n_1]x^*[n_2]\} \quad (7)$$

where  $x^*$  is the complex conjugate of  $x$ . For a stationary random process, the autocorrelation depends only on the time-difference or lag index,  $n_1 - n_2$  or  $m$ . The autocorrelation of a stationary discrete random process is thus given by

$$r_{xx}[m] = \mathcal{E}\{x[n+m]x^*[n]\} \quad (8)$$

To describe how the variance of a random process is distributed with frequency, the Power Spectral Density (PSD) is computed. For stationary signals the PSD is given by Eq. (9), which is bandlimited to  $\pm 1/(2T)$ , and is defined as the discrete-time Fourier transform of the autocorrelation function.

$$P_{xx}(f) = T \sum_{m=-\infty}^{\infty} r_{xx}[m] \exp(-j2\pi fmT) \quad (9)$$

The inverse discrete-time Fourier transform of Eq. (9) yields an expression for the autocorrelation function

$$r_{xx}[m] = \int_{-\frac{1}{2T}}^{\frac{1}{2T}} P_{xx}(f) \exp(j2\pi fmT) df \quad (10)$$

If the autocorrelation function given in Eq. (10) is evaluated at zero lag, then an expression for the average signal power of a random stationary process results:

$$\text{Average Signal Power} = r_{xx}[0] = \int_{-\frac{1}{2T}}^{\frac{1}{2T}} P_{xx}(f) df \quad (11)$$

Equation (11) indicates that the area under the PSD is the average power, and emphasizes that the PSD is a density function that represents the distribution of power with respect to frequency.<sup>8</sup>

### Application

In applying the algorithms, several system conditions required consideration in order to ensure that the algorithms would not erroneously indicate an engine fault. These conditions were sensor failure, propellant tank venting and pressurization, and propellant transfer.

Both nominal and anomalous test firings have experienced sensor failures. Sensor failure detection methods must be employed before, or concurrently, with safety monitoring algorithms in order to eliminate the possibility of a sensor failure being interpreted as an engine problem. For this investigation, all parameters exhibiting sensor problems were removed prior to the application of the two algorithms.

Some test firings have included propellant transfer from barges, or propellant tank venting and pressurization. For several parameters, these processes introduce transient excursions that are not due to power level transitions. Figure 1(a) illustrates the effect of venting followed by pressurization on the HPOP inlet pressure for test firing A2-463. The decrease and subsequent increase observed in the signal correspond directly to the venting and pressurization processes. Figure 1(b) shows the Main Combustion Chamber (MCC) controller reference pressure for the same test. The controller reference pressure has been included so that the effects due to power level transitions can be differentiated from the effects due to tank venting and pressurization. In a test without venting or pressurization, the curves in Figs. 1(a) and (b) would have similar shapes.

### Time Series Algorithm

AR models were computed for the nine parameters indicated in Table 1. The Parameter Identification (PID) numbers listed in Table 1 are used to label the parameters on SSME data tapes. The additional parameters given in Table 1 displayed excursions or non-stationary

behavior as compared to the model computation interval, and thus did not satisfy the stationary requirement of the time series algorithm. In many cases, this non-stationary behavior was due to tank venting, pressurization, or propellant transfer. In order to apply the time series algorithm to additional parameters, a method which would remove the transient effects caused by these processes is required.

The AR and ARMA models were created during 4 sec of engine operation in which the parameter exhibited steady-state or stationary behavior. Not all parameters achieved steady-state behavior at the same time following the scheduled completion of a transient. Therefore, a safety factor of at least 2 sec was allowed prior to model construction. This allowed models for all parameters of a given test firing to be computed over the same interval. For ease of computation and interpretation, the mean was removed from the data prior to model construction. The 4-sec window represented a trade-off between model computation time and model prediction accuracy. A larger computation window increased the ability of the model to accurately predict future signal behavior; however, a larger window also increased the time during which the time series algorithm was not available for safety monitoring.

Each model was evaluated using four criteria. These criteria were (1) monitoring the FPE, (2) computing the poles and zeros of the model and checking for stability and overlap, (3) comparing the actual frequency response to that of the model, and (4) ensuring that the residual autocorrelation function did not exceed the confidence interval. In applying these criteria to AR and ARMA models of various orders, it was found that the autoregressive model of order five, AR[5], provided the most consistent, adequate representation of the data. This concurred with the previously reported AR model order applied to SSME data.<sup>4</sup> In general, it was found that ARMA models introduced spurious information into the model frequency response. Also, ARMA models experienced stability problems, and had added computational burden. AR models of an order less than five successfully described only a minority of the parameters. As the AR model order was increased to values greater than five, marginal improvements in the FPE and the residual autocorrelation function were sometimes observed, but the frequency response of the model and data began to diverge.

Once a model had been created, it was used to predict the future behavior of the signal. The 4-sec window was moved forward in time in 1-sec increments; thus, any two adjacent windows overlapped by

75 percent. For each window the autocorrelation function of the residuals was computed for lags between 0 and 25. One lag was equivalent to one sampling interval or 40 msec. When implemented in hardware, the 1-sec time increment could be decreased to the 40 msec sampling rate to improve the failure detection capability of the algorithm.

Due to the highly dynamic nature of the system, the residual confidence interval was often exceeded for the A2 nominal tests. This necessitated thresholds to be established to prevent incorrect failure indications. The thresholds given in Table 2 represent the maximum absolute value of the residual autocorrelation function for all of the A2 nominal tests at either 104 percent RPL or 109 percent RPL. Although the models generated at 104 percent RPL were often adequate in describing the data at 109 percent RPL, both models were computed in order to base the thresholds on a larger data set. If the residual autocorrelation function for the model computation window fell outside the confidence interval, the model was not included in the threshold determination. When used in the failure detection mode, failure of an autocorrelation function to fall within the threshold interval given in Table 2 resulted in a failure indication.

In applying the time series algorithm to parameters that were susceptible to venting and pressurization, extremely high thresholds were required to ensure no false failure indications. This was expected since these parameters exhibited non-stationary behavior. For example, the Low Pressure Oxidizer Pump (LPOP) shaft speed (PID 30) required a threshold of 0.9 on a scale of one. A threshold of this magnitude clearly indicates that the time series algorithm is not an appropriate failure indicator.

#### Average Signal Power Algorithm

The average signal power of various SSME parameters was determined by computing the autocorrelation at zero lag, as given by Eq. (11), for the parameters listed in Table 1. This equation assumes that the signal is stationary over the computation interval. Although some parameters exhibited overall non-stationary trends, stationary behavior was achieved during the 2-sec computation interval. Therefore, the computation of the average signal power using the autocorrelation function was valid.

The average signal power calculations were performed over 2-sec, 50 percent overlapping windows for the A2 nominal test firings at both 104 percent RPL

and 109 percent RPL. In order to base the threshold calculations on a larger data set, both engine power levels were used in the determination of the failure indication thresholds. This was possible since the average signal power was not consistently higher at either power level. The 2-sec window and 1-sec time increment were selected for ease of computation. In a hardware implementation, the window could be decreased to minimize the initial computation time during which the algorithm would not be available for failure detection. Also, the time increment could be decreased to improve the failure detection capability of the algorithm. As in the time series algorithm, the mean was removed from the data prior to the application of the algorithm.

The average and three standard deviations of the average signal power were computed for all seven A2 nominal firings at both engine power levels. To calculate the thresholds, these values were combined as shown in Eq. (12). The expectation operator,  $\mathcal{E}$ , used in Eq. (12) was previously defined in Eq. (6).

$$\text{threshold} = \left[ \frac{1}{2 \cdot 7} * \sum_{i=1}^{2 \cdot 7} \mathcal{E}(\text{average power}_i) + \frac{1}{2 \cdot 7} * \sum_{i=1}^{2 \cdot 7} 3 * \text{standard deviation}_i \right] * \text{safety factor} \quad (12)$$

A factor of safety from 1.5 to 3.5 was needed to ensure no false failure indications for the A2 nominal firings. The safety factors reflected the variations in signal behavior observed over these firings. The thresholds and safety factors are given in Table 2. When used in the failure detection mode, failure of the average signal power of a parameter to fall beneath its threshold results in a failure indication.

For some of the parameters sensitive to venting and pressurization, the required safety factors were greater than 2.5. These parameters were the HPOT discharge temperatures (PIDs 233 and 234) and the Preburner Boost Pump (PBP) discharge temperature (PID 94). The high safety factors were attributed to the transient behavior introduced by the venting and pressurization processes. As with the time series algorithm, the average signal power algorithm could be applied to a larger set of parameters if the effects due to these processes could be removed. In addition, the HPFP shaft speed (PID 260) also required a large safety factor. This was attributed to the extremely noisy signal observed for this parameter. The larger safety factors decreased the

ability of the average signal power algorithm to detect engine anomalies, thereby degrading the effectiveness of the algorithm. Thus, the parameters which required factors of safety greater than 2.5 were not used for failure detection.

### Results and Discussion

Failure indication thresholds were established by applying the time series and average signal power algorithms to seven A2 nominal tests. Four anomalous firings and one A1 nominal firing were tested using the thresholds given in Table 2.

The four anomalous test firings analyzed, A2-249, A1-340, A1-364, and A1-436, were all High Pressure Fuel Turbopump (HPFTP) failures. Detailed failure summaries may be found in Ref. 2. These firings were chosen for two reasons: (1) the failures occurred during steady-state operation of the engine and (2) the firings exhibited failure indications before redline cutoff values were attained. In addition, a more recent nominal firing, A1-618, was also tested against the thresholds to ensure that false failure indications would not occur. Although only HPFTP anomalies were considered, performance parameters from many parts of the engine were selected. The high degree of interdependence among engine components typically causes a failure in one component to quickly manifest itself throughout the engine.

In applying the time series algorithm to the parameters indicated in Table 1, a series of plots was developed to evaluate the validity of the computed models. Figure 2 displays an example of the plots necessary in determining validity of the AR[5] model for the HPFP discharge pressure for test A2-463. Figure 2(a) displays the five zeros of the model, along with the uncertainties in their locations. The uncertainties are calculated for both the real and imaginary parts; thus, the uncertainty in location of the real zero is given by a line. As required for stability, the zeros all lie within the unit circle, and their uncertainty regions do not overlap or cross the unit circle. Figure 2(b) compares the trends in the frequency response of the model with the trends in the frequency response of the actual data. As can be seen, these two curves respond similarly with frequency. Finally, the autocorrelation function of the residuals for the 4-sec model computation window is given in Fig. 2(c). The autocorrelation of the residuals is well within the confidence interval for lags greater than zero, indicating that the residuals are random noise as required. These figures demonstrate that the AR[5] model is a valid predictor of the HPFP discharge pressure.

Figure 3 is an example of the application of the time series algorithm to an anomalous test firing. The HPFP discharge pressure for test A1-340 is the parameter shown. Within each 4-sec window, the autocorrelation function of the residuals is computed, and the maximum value exceeding the confidence interval is plotted as a function of time. The failure indication thresholds for the HPFP discharge pressure are also indicated in Fig. 3. The parameter exceeds the thresholds seven times. These times correspond to the events detailed in the failure summary report for this test firing. During test A1-340, the Turn/Around duct inner wall fractured at 20.6 sec and major ruptures occurred at 290 sec.<sup>2</sup> Figure 3 also displays the tendency of the residuals to exceed the thresholds for an interval of time, and then subsequently fall back between the thresholds. This can be attributed to attempts, by the engine, to compensate for anomalous occurrences and return to a nominal mode of operation.

Table 3(a) lists a majority of the failure indication times obtained by applying the time series algorithm to the four anomalous test firings. The values listed indicate the times, in seconds from start, at which a given parameter exceeded its failure indication thresholds. In some cases, the residual autocorrelation function confidence interval was exceeded for the model computation window. Such models became biased estimators of future behavior and were therefore considered invalid. The parameters affected by this phenomenon were the mixture ratio (PID 8) for test firings A1-340 and A1-364, and the Low Pressure Fuel Pump (LPFP) shaft speed (PID 32) for test firing A1-364. The question of model validity presents a unique implementation concern for the time series algorithm. A model can be checked in real-time; however, it cannot be recomputed using a different order number. Thus, the failure detection capability of the time series algorithm would be compromised as the number of parameters with invalid models increased.

When space permitted, all of the times at which the time series algorithm thresholds were exceeded are included in Table 3(a). For some parameters, the times that the thresholds were exceeded were too numerous to list completely. For these parameters, the first failure indication times are given, as well as those times which were in closest agreement with the failure indication times of the other parameters. This was done to show agreement among the parameters of a given test firing and to provide insight into the progression of engine problems during the test firing. For example, test A2-249 showed agreement among several parameters at approximately 398 sec. This could be in response to the

melting of the Kel-F ring documented at 374 sec.<sup>2</sup> However, the MCC pressure (PID 130), the HPFP shaft speed (PID 260) and the LPFP shaft speed (PID 32) clearly gave earlier indications of abnormal engine behavior at 123, 156, and 146 sec, respectively. The failure summary report indicated that cavitation of the HPFP commenced at 108 sec due to the increased pump inlet temperatures caused by propellant transfer.

For each anomalous firing, two types of failure indication times for the time series algorithm were extracted from Table 3(a). The first type was the first time at which any parameter of a given test firing exceeded its failure indication thresholds. The first failure indication times for tests A2-249, A1-340, A1-364, and A1-436 were 123, 21, 137 and 176 sec, respectively. These times were at least 250 sec earlier than the corresponding redline cutoff times which are also given in Table 3(a). The second type of failure indication time is the first time at which two or more parameters simultaneously indicated a failure. Table 3(b) lists these times for the four anomalous firings, along with the number of parameters in agreement. The first simultaneous failure indication times occurred at least 50 sec prior to the redline cutoff times. The first simultaneous failure indication times are significant since agreement between two or more parameters increases the likelihood that an engine problem has occurred. In the absence of a thorough sensor signal validation package, agreement among several sensors minimizes the chance of a sensor failure being interpreted as an engine problem. On the other hand, requiring multiple parameters to exceed the thresholds simultaneously reduces the ability of the algorithm to detect failures before they have propagated through the system. For the anomalous firings studied, either of the time series algorithm failure indication times could have alerted engine operators and prevented the progression of these failures to catastrophic levels.

An example of the computation of the average signal power for a nominal test firing is given in Fig. 4. The interval over which the average signal power was computed for the HPFP discharge pressure for test firing A2-457 is given in Fig. 4(a), and the resulting average signal power is given as a function of time in Fig. 4(b). The fluctuations in the average signal power were observed in all of the nominal firings and were considered normal. The fluctuations were taken into account in calculating the thresholds for the parameters. The HPFP discharge pressure had a threshold of 436, well above the maximum average signal power shown in Fig. 4(b).

An example of the application of the average signal power algorithm to an anomalous test firing is given in Fig. 5. Figure 5(a) shows the interval over which the average signal power was computed for the HPFP discharge pressure for test firing A1-340. Figure 5(b) displays the resulting average signal power, as a function of time. The failure indication threshold calculated from the A2 nominal firings is also shown. As can be seen, increases in the average signal power concur with the deviations observed in the signal. The maximum average signal power for test A1-340 is almost an order of magnitude greater than the maximum average signal power for a nominal firing. Figures 3 and 5(b) show that, for the HPFP discharge pressure, the thresholds for both algorithms were exceeded at approximately the same times. However, the average signal power exceeded its threshold by a much larger percentage than did the time series algorithm. This may be critical if testing against additional nominal firings required the thresholds to be increased.

Table 4(a) summarizes the application of the average signal power algorithm to the four anomalous test firings. The values listed indicate the times, in seconds from start, at which a given parameter exceeded its average signal power threshold. Most of the times at which the thresholds were exceeded were included in Table 4(a) to show agreement among parameters of a given test firing and to demonstrate the progression of the failure during the test firing. For example, test firing A1-340 showed agreement among five parameters at 21 sec and eight parameters at 290 sec. As stated previously, this concurred with the failure investigation summary report which states that the Turn/Around duct inner wall fractured at 20.6 sec and major ruptures occurred at 290 sec.<sup>2</sup>

The two types of failure indication times determined for the time series algorithm were also considered for the average signal power algorithm. The first failure indications for the average signal power algorithm for tests A2-249, A1-340, A1-364, and A1-436 were 61, 21, 149, and 32 sec, respectively. These times were at least 240 sec earlier than the corresponding redline cutoff times which are given in Table 4(a). The first time at which two or more parameters exceeded their thresholds are given for each anomalous test firing in Table 4(b), along with the number of parameters which were in agreement. Generally, the first simultaneous failure indication times were substantially earlier than the redline cutoff times. As with the time series algorithm, the simultaneous indication of a fault by two or more parameters increases the likelihood that an actual

engine problem has occurred and minimizes the chance of erroneous failure indications.

A comparison between Tables 3(a) and 4(a) indicates that the average signal power algorithm detected an engine problem 62 sec earlier than the time series algorithm for firing A2-249 and 144 sec earlier for firing A1-436. For test A1-340, the two approaches had identical first failure indication times, and for test A1-364, the time series algorithm indicated a failure condition 12 sec earlier than the average signal power algorithm. The HPFP shaft speed (PID 260) provided the earliest failure indication time for test A1-364. This parameter was not evaluated by the average signal power method due to the high safety factor required. For all four anomalous firings, the HPFP shaft speed provided early failure indications using the time series algorithm. This was expected since the four anomalous firings considered in this study were all HPFTP failures. The average signal power was computed for six parameters to which the time series algorithm was not applied. With the exception of the LPOP shaft speed (PID 30), these additional parameters provided failure indications earlier than the redline cutoff times. For test A2-249, one of the additional parameters, the HPFT discharge temperature (PID 231), gave the earliest failure indication time.

By comparing Tables 3(b) and 4(b), it is evident that the average signal power algorithm had a greater number of parameters contributing to the first simultaneous failure indication time for each anomalous test firing. A larger number of concurring parameters increased confidence in the ability of the average signal power algorithm to detect actual engine failures. The two algorithms had an identical first simultaneous failure indication time for test A2-249. For tests A1-340 and A1-436, the average signal power algorithm gave times that were 270 and 321 sec earlier than the time series algorithm, respectively. For A1-364, the time series algorithm gave a time which was 233 sec earlier. Simultaneous failure indication times were explored to demonstrate the need for shutdown recommendation criteria in addition to failure indication thresholds. Failed sensors are of particular concern since no thorough sensor screening techniques currently exist on the SSME. It is vital that an algorithm not issue a shutdown command because of a failed sensor. The shutdown recommendation criteria must be established to ensure no erroneous failure indications on a nominal test, even in the event of failed sensors.

An additional nominal firing, A1-618, was tested using the time series and average signal power thresholds developed in this study. This was done to increase confidence in the thresholds of the two algorithms. Neither algorithm produced any failure indications for this test firing. An extensive amount of testing against additional nominal test firings is required to validate and refine the proposed thresholds, and to establish shutdown recommendation criteria based on the thresholds. Testing against additional anomalous firings would further define the capabilities of the two algorithms.

### Concluding Remarks

The earliest possible detection of anomalous behavior during a firing of the SSME is critical. This investigation determined the ability of two algorithms to detect the onset of engine faults during steady-state operation of the engine. Time series techniques had been previously studied. In this investigation, the time series algorithm used fifth order AR models to predict the future behavior of parameters based on their past behavior. The average signal power algorithm was a newly proposed SSME failure detection algorithm. It consisted of computing and tracking variations in the average signal power with time. The same seven A2 nominal tests were used to develop parameter fault indication thresholds for both algorithms. These thresholds were applied to four anomalous firings and one additional nominal firing.

For all four anomalous test firings, both the time series algorithm and the average signal power algorithm provided first failure indication times and first simultaneous failure indication times that were significantly earlier than the redline cutoff times. For all four firings, the average signal power algorithm had a larger number of parameters contributing to the first simultaneous failure indication times. This is significant since agreement between several parameters increases the likelihood that an engine problem has occurred, and minimizes the chance of false failure indications. Confidence in both algorithms was further established when the thresholds did not produce any erroneous failure indications for the additional nominal firing.

The average signal power algorithm had several advantages over the time series algorithm. A longer window was needed for the time series algorithm to ensure model validity. The longer window increased the time during which this algorithm was not available for failure detection. Even with this longer window several

of the calculated models were invalid. The question of model validity presented a unique implementation concern for the time series algorithm. A model can be checked in real-time; however, it cannot be recomputed using a different order number. A large number of invalid models on a test firing would compromise the failure detection capability of the time series algorithm. The average signal power algorithm was applicable to a larger set of performance parameters because it did not depend as rigidly on the stationary behavior of the signal. Stationary behavior was achieved over the 2-sec interval used to compute the average signal power, allowing this algorithm to be applied to parameters exhibiting overall non-stationary trends.

Some types of sensor failures would cause both of the algorithms to exceed their thresholds. This indicates the need for sensor failure detection methods in order to eliminate the possibility of a sensor failure being interpreted as an engine problem. Both algorithms were affected by engine processes such as tank venting and pressurization, although the average signal power algorithm was less sensitive because it did not involve the computation of a model. Both algorithms could be applied to a larger set of performance parameters if a technique were developed to remove the transient effects caused by these processes.

The failure indication thresholds developed in this investigation must be tested extensively against additional nominal and anomalous firings. The nominal tests would refine the thresholds to ensure no erroneous failure indications, and the anomalous test firings would further demonstrate the capabilities and limitations of the algorithms. Finally, shutdown recommendation criteria must be developed for the algorithms.

### Acknowledgment

This work was supported by the NASA Lewis Research Center under contract NAS3-25266 with Larry P. Cooper as monitor.

### References

1. Cikanek, H.A. Characteristics of Space Shuttle Main Engine Failures. *AIAA Paper 87-1939*, June 1987.
2. Taniguchi, M.H. *Failure Control Techniques for the SSME, Phase I Final Report*. NASA CR-179224, 1986.

3. Taniguchi, M.H. *Failure Control Techniques for the SSME, Phase II Final Report*. NASA CR-179231, 1987.
4. Hawman, M.H., Galanitis, W.S., Tulpule, S., and Mattedi, A. *Framework for a Space Shuttle Main Engine Health Monitoring System, Final Report*. NASA CR-185224, May 1990.
5. Nemeth, E. *Health Management System for Rocket Engines, Final Report*. NASA CR-185223, June 1990.
6. Braun, S., ed. *Mechanical Signature Analysis: Theory and Applications*. London: Academic Press, 1986.
7. Ljung, L. *System Identification: Theory for the User*. Englewood Cliffs, NJ: Prentice Hall, Inc., 1987.
8. Marple, S.L. *Digital Spectral Analysis with Applications*. Englewood Cliffs, NJ: Prentice Hall, Inc., 1987.

PID No.	Parameter Name	Time Series	Ave. Power
8	Mixture Ratio	x	x
17	MCC Coolant Discharge Press.	x	x
24	MCC Hotgas Injector Press.	x	x
30	LPOP Shaft Speed		x
32	LPFP Shaft Speed	x	x
52	HPFP Discharge Pressure	x	x
58	Fuel Preburner Chamber Press.	x	x
59	PBP Discharge Pressure		x
90	HPOP Discharge Pressure	x	x
94	PBP Discharge Temperature		x
130	MCC Pressure	x	x
203	HPFP Inlet Pressure		x
209	HPOP Inlet Pressure		x
231	HPFT Disharge Temp. A		x
232	HPFT Disharge Temp. B		x
233	HPOT Discharge Temp. A		x
234	HPOT Discharge Temp. B		x
260	HPFP Shaft Speed	x	x

x - algorithm applied

Table 1. Description of PID numbers used with time series and average signal power algorithms.

PID No.	Time Series Thresholds	Average Power	
		Thresh- olds	Safety Factors
8	$\pm .60$	.00112	1.5
17	$\pm .50$	200	1.5
24	$\pm .50$	125	1.5
30	--	1598	2.5
32	$\pm .55$	2509	1.5
52	$\pm .50$	436	1.5
58	$\pm .60$	232	1.5
59	--	911	1.5
90	$\pm .475$	268	1.5
94	--	.04	3.0
130	$\pm .50$	47	1.5
203	--	4	1.5
209	--	6	1.5
231	--	32	2.0
232	--	38	2.5
233	--	154	3.5
234	--	104	3.5
260	$\pm .65$	550000	3.5

Table 2. Thresholds calculated from the nominal test firings for the time series algorithm and the average signal power algorithm, and safety factors for the average signal power algorithm.

Test No. PID No.	A2-249	A1-340	A1-364	A1-436
8	a	c	c	a
17	398-401	291-293	154,245 387-90	176,242
24	a	290	388-90	a
32	146-8,... 224- 35,...304-5,... 390-7,402-10,.. 421-49 d	280,291-93	c	369-70,377-9 394-6,414 432-33
52	398-399	21-3,291-3 380	389-390	a
58	b	b	387-90	a
90	401	b	203,245,302 387-390	a
130	123,306-307 399	291-93	387-90	a
260	156-227 229-32,430-1 434	56-65,... 99-247,... 276-9 d	137,142-56,... 300-75,377, 390-1d	203,205,... 353-423,425- 511,...588-9 d
Redline Cutoff Time	450.58	405.5	392.15	611.06

- a threshold not exceeded
- b failed sensor
- c model not valid
- d times too numerous to list completely

Table 3a. The times, in seconds from start, at which the four anomalous test firings exceeded the time series algorithm failure indication thresholds.

Test No.	A2-249	A1-340	A1-364	A1-436
First Simultaneous Failure Indication Time	398	291	154	369
Number of Concurring Parameters	2	4	2	2

Table 3b. The first times, in seconds from start, at which two or more parameters simultaneously indicated failure, and the number of parameters which exceeded their thresholds at these times.

Test No. PID No.	A2-249	A1-340	A1-364	A1-436
8	a	22,290-291	a	a
17	399,413	21-2,290-1 357-358	387-388	a
24	a	21-2,290-2, 358	a	32-3,..47-8,.. 72-8,83-4,90-1 ..117-9,..201-2 221-3,..231,.. 319-20,..467-8 <sup>c</sup>
30	a	b	a	a
32	a	290-291	a	a
52	398-399,413	21-2,290-1 357-358	387-388	a
58	b	b	387-388	a
59	106,399	21,290-291	387	48-9,72-3,90-1 119,202,221-3, ..,319,343-4,.. 484,..543,.. 580 <sup>c</sup>
90	a	b	a	49
130	398-399	21-2,290-1 357-358	387-388	48-9,72-3,91 150,201-2,241 344,461,475 484-485
203	a	290-291	a	a
209	88-89,125-126	a	211	a
231	61,123,..,398- 400,410,413,.. 431-4,443-6 449 <sup>c</sup>	b	149,154,159 182-3,219,244 316-7,335, 387-388	205,319
232	137,327,409 412-3,415-6 429,433-6,447	a	387-388	84,91,176,201 231,297,373 402-4,484,512 543,603-4
Redline Cutoff Time	450.58	405.5	392.15	611.06

a threshold not exceeded

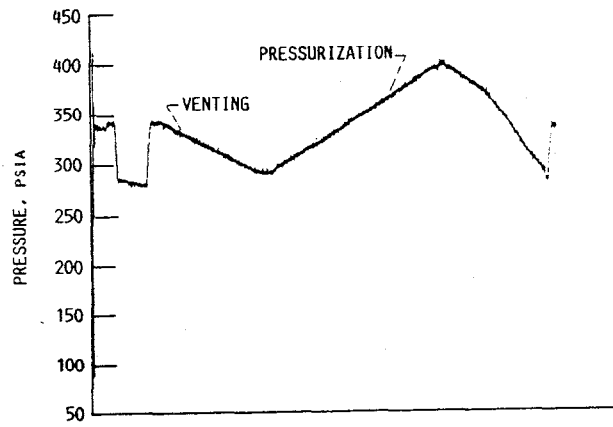
b failed sensor

<sup>c</sup> times too numerous to list completely

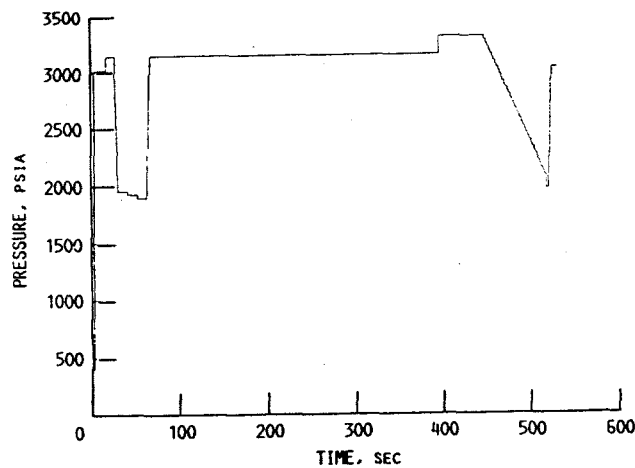
Table 4a. The times, in seconds from start, at which the four anomalous test firings exceeded the average signal power algorithm failure indication thresholds.

Test No.	A2-249	A1-340	A1-364	A1-436
First Simultaneous Failure Indication Time	398	21	387	48
Number of Concurring Parameters	3	5	7	3

Table 4b. The first times, in seconds from start, at which two or more parameters simultaneously indicated failure, and the number of parameters which exceeded their thresholds at these times.

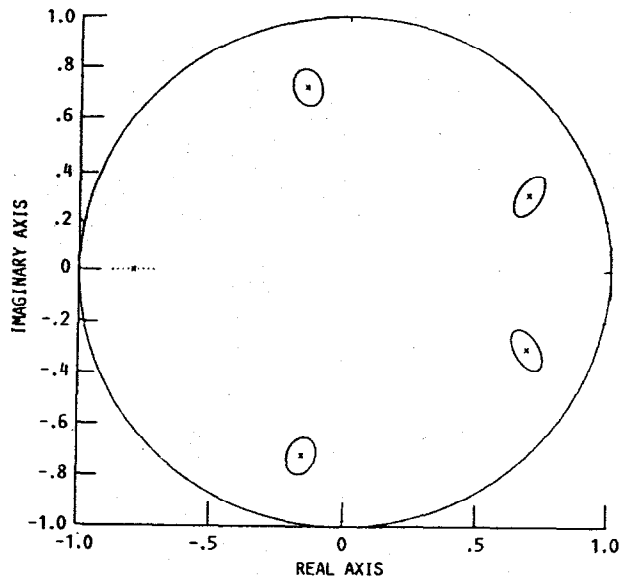


(a) HPOP INLET PRESSURE FOR TEST FIRING A2-463.

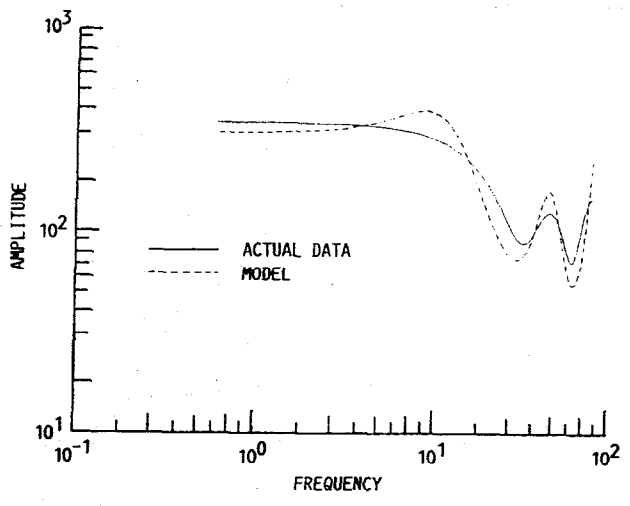


(b) MCC CONTROLLER REFERENCE PRESSURE FOR THAT TEST.  
(CONTROLLER REFERENCE PRESSURE SHOWS SCHEDULED POWER LEVEL TRANSITIONS.)

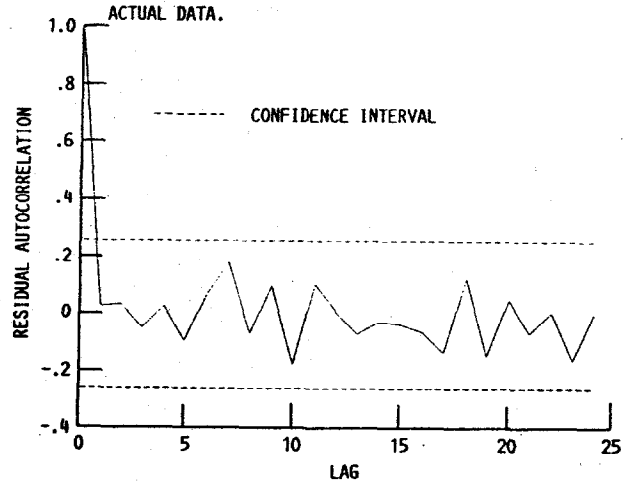
FIGURE 1. - EFFECT OF TANK VENTING FOLLOWED BY PRESSURIZATION.



(a) ZEROS OF THE MODEL WITH UNCERTAINTIES IN LOCATION.



(b) COMPARISON BETWEEN FREQUENCY RESPONSE OF MODEL AND ACTUAL DATA.



(c) AUTOCORRELATION FUNCTION OF THE RESIDUALS FOR THE MODEL COMPUTATION WINDOW.

FIGURE 2. - PLOTS USED TO DETERMINE THE VALIDITY OF THE AR(5) MODEL FOR THE HPFP DISCHARGE PRESSURE FOR TEST A2-463.

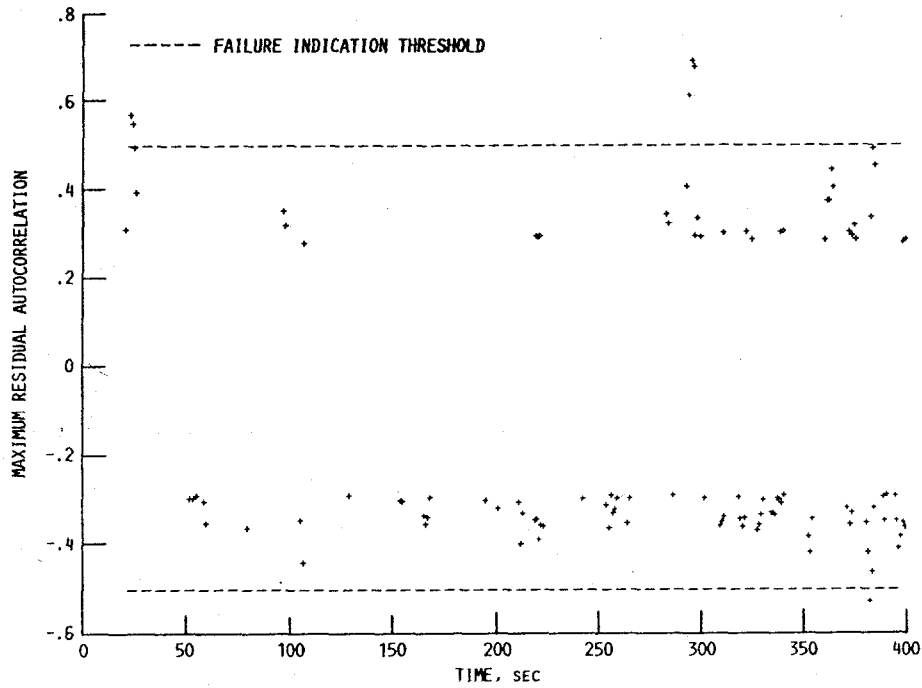
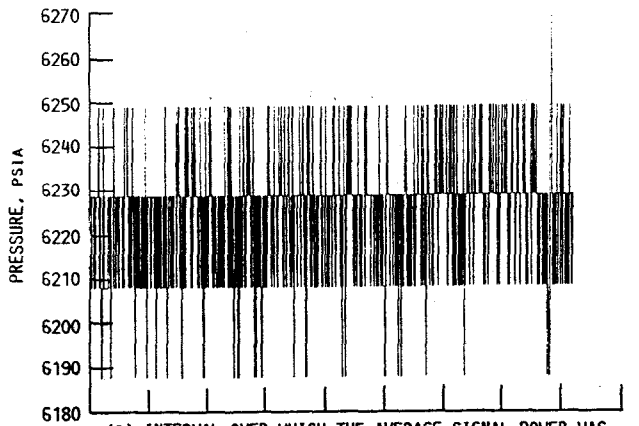
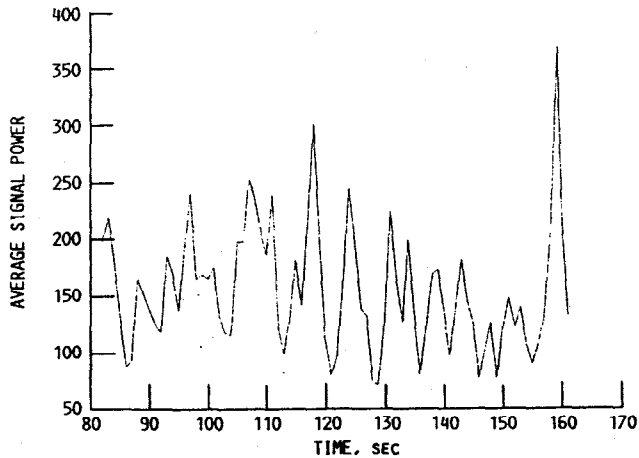


FIGURE 3. - APPLICATION OF THE TIME SERIES ALGORITHM THRESHOLDS TO THE HPFP DISCHARGE PRESSURE FOR TEST A1-340.

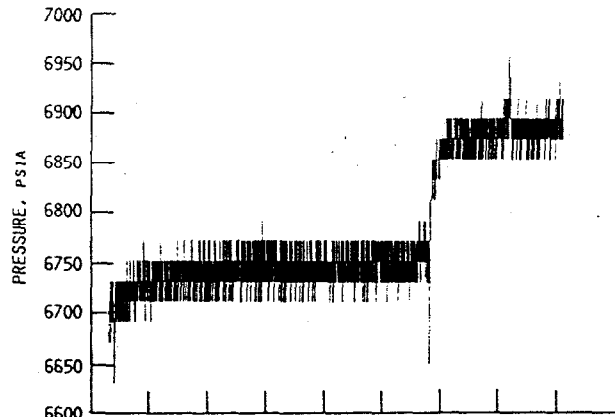


(a) INTERVAL OVER WHICH THE AVERAGE SIGNAL POWER WAS COMPUTED.

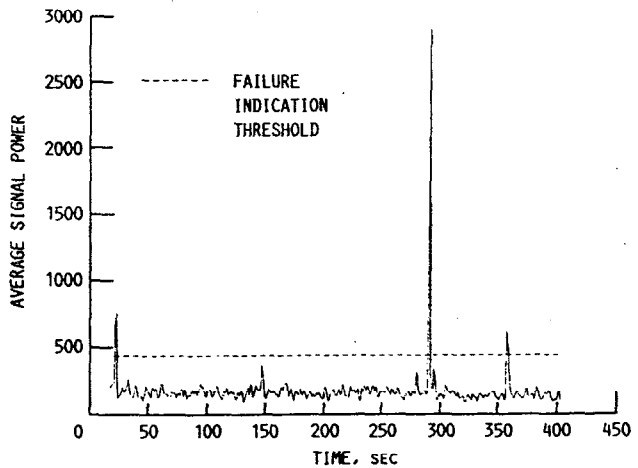


(b) AVERAGE SIGNAL POWER FOR THAT INTERVAL.

FIGURE 4. - COMPUTATION OF THE AVERAGE SIGNAL FOR THE HPFP DISCHARGE PRESSURE FOR NOMINAL TEST A2-457.



(a) INTERVAL OVER WHICH THE AVERAGE SIGNAL POWER WAS COMPUTED.



(b) AVERAGE SIGNAL POWER FOR THAT INTERVAL WITH THE FAILURE INDICATION THRESHOLD.

FIGURE 5. - APPLICATION OF THE AVERAGE SIGNAL POWER ALGORITHM TO THE HPFP DISCHARGE PRESSURE FOR TEST A1-340.